



HAL
open science

Experimental and computational insights into the mechanism of destabilization of poly(acrylic acid)-capped silver nanoparticles induced by weak conjugate bases

Marin Kovačić, Irena Ivanišević, Antonia Ressler, Panaghiotis Karamanis

► To cite this version:

Marin Kovačić, Irena Ivanišević, Antonia Ressler, Panaghiotis Karamanis. Experimental and computational insights into the mechanism of destabilization of poly(acrylic acid)-capped silver nanoparticles induced by weak conjugate bases. *Colloids and Surfaces A: Physicochemical and Engineering Aspects*, 2024, 690, pp.133739. 10.1016/j.colsurfa.2024.133739 . hal-04580732

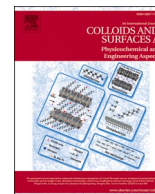
HAL Id: hal-04580732

<https://univ-pau.hal.science/hal-04580732v1>

Submitted on 20 May 2024

HAL is a multi-disciplinary open access archive for the deposit and dissemination of scientific research documents, whether they are published or not. The documents may come from teaching and research institutions in France or abroad, or from public or private research centers.

L'archive ouverte pluridisciplinaire **HAL**, est destinée au dépôt et à la diffusion de documents scientifiques de niveau recherche, publiés ou non, émanant des établissements d'enseignement et de recherche français ou étrangers, des laboratoires publics ou privés.



Experimental and computational insights into the mechanism of destabilization of poly(acrylic acid)-capped silver nanoparticles induced by weak conjugate bases

Marin Kovačić^{a,*}, Irena Ivanišević^{a,b}, Antonia Ressler^{a,c}, Panagiotis Karamanis^d

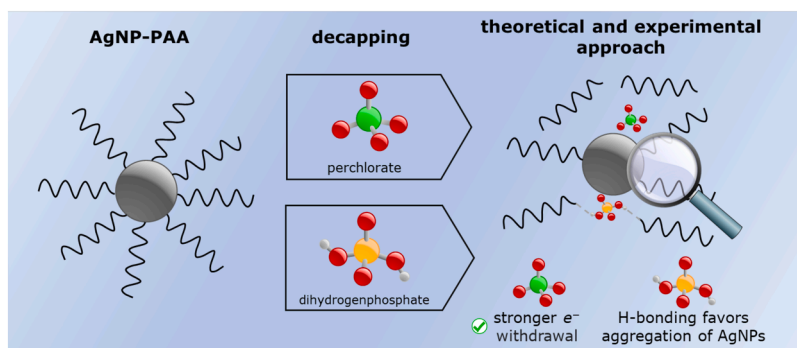
^a University of Zagreb, Faculty of Chemical Engineering and Technology, Trg Marka Marulića 19, Zagreb HR-10000, Croatia

^b Ruder Bošković Institute, Division of Physical Chemistry, Bijenička cesta 54, Zagreb HR-10000, Croatia

^c Tampere University, Faculty of Engineering and Natural Sciences, Korkeakoulunkatu 6, P.O. Box 589, Tampere FI-33014, Finland

^d CNRS/UNIV Pau et Pays de l'Adour, Institut Des Sciences Analytiques et de Physico-Chimie pour l'environnement et les Matériaux – UMR5254, Hélioparc Pau Pyrénées, 2 avenue du Président Pierre Angot, FR-64053 Pau Cedex 09, France

GRAPHICAL ABSTRACT



ARTICLE INFO

Keywords:

AgNP
DFT
Poly(acrylic acid)
Spectroscopic titration
Weak conjugate base

ABSTRACT

Herein we report a systematic study of the effects of H_2PO_4^- and ClO_4^- on the stability of poly(acrylic acid)-capped silver nanoparticles (PAA-AgNPs). Spectroscopic titration revealed that a smaller amount of ClO_4^- is required to detach PAA, and a blue-shift in surface plasmon resonance (SPR) was observed relative to H_2PO_4^- , owing to its electron accepting nature which leads to a weakening of the PAA-AgNP donor bond. Experimental observations were supported by DFT calculations, which revealed that complexation of AgNPs with ionized PAA, H_2PO_4^- and ClO_4^- is mediated by the electron affinity of the AgNP and the conjugated bases. Electron donation by the weak acids leads to the weakening of the PAA-AgNP donor bond, whereby ClO_4^- contributes more to the destabilization of the PAA capped AgNPs due to its greater electron affinity. Additionally, H_2PO_4^- can form hydrogen bonds with PAA, which promotes the formation of aggregates. Moreover, DFT calculations have shown that the structure of the model Ag_{14} cluster is significantly distorted in the presence of H_2PO_4^- , more so than in the case of ClO_4^- . The findings are supported by the experimental quantification of residual PAA by differential scanning calorimetry and solid-state total organic carbon analysis (SSM-TOC), and powder X-ray diffraction (XRD).

* Corresponding author.

E-mail address: mkovacic@fkit.unizg.hr (M. Kovačić).

<https://doi.org/10.1016/j.colsurfa.2024.133739>

Received 6 December 2023; Received in revised form 24 January 2024; Accepted 15 March 2024

Available online 15 March 2024

0927-7757/© 2024 Published by Elsevier B.V.

1. Introduction

Advances in nanotechnology, and particularly metallic nanomaterials, have led to their rapidly increasing applications in a variety of fields [1–3]. Among metallic nanomaterials, silver nanoparticles (AgNPs) are the most widely used type [4–6]. Precise tuning of the surface properties is a major challenge in the development of nanosilver materials, as these properties are paramount from an application standpoint. A crucial problem faced by almost all practical applications of AgNPs is related to their insufficient stability in dispersion, i.e., their tendency to form aggregates. Unlike relatively chemically inert bulk silver, AgNPs are highly reactive due to their large specific surface area. Thus, AgNPs have a spontaneous tendency to minimize the total surface energy of the colloidal system by forming larger particles. Aggregation is thermodynamically governed by the favourable energy difference between the enthalpy of crystallization and the entropy and the hydration/solvation energy of the individual colloidal particles [7]. When repulsive forces are introduced between individual AgNPs, e.g., Coulombic repulsion and/or steric effects due to the attachment of bulky ligands on their surface, the probability of aggregation decreases with an increasing potential barrier height. In addition, strong long-range repulsive forces between AgNPs should lead to kinetically stable dispersions, preventing and the particles to aggregate over extended periods of time. In addition to the attractive and electrical repulsive van der Waals forces (DLVO theory), an important kinetic parameter in random particle-solvent collisions is Brownian motion [8]. Since AgNPs are often associated with non-covalently or covalently bonded ligands (i.e., ions, surfactants, peptides, lipids, nucleic acids, polymers), in dispersion or powder form, they are a versatile tool [9] for applications such as drug delivery [10], (bio)sensing [11], catalysis [12], printable electronics [13] and water purification systems [14]. A detailed understanding of the aggregation mechanism responsible for the formation of stable nanoparticles and larger clusters is of great importance, as aggregation drastically changes the particle reactivity, mobility, persistence in the environment and toxicity of the particles.

Polyelectrolytes, i.e., polymer macromolecules bearing positively or negatively charged ionizable groups, provide electrostatic stabilization, acting as attractive agents for nanoparticle stabilization. Poly(acrylic acid) (PAA) is a weak anionic polyelectrolyte used in industry for superabsorbent materials and also as a protective agent in the preparation of silver nanoparticles by chemical reduction [15]. The ability of PAA to adsorb and adhere to the surface of silver nanoparticles controls the structure/activity relationship (formation of cluster size and geometry), i.e., stabilization of the nano-colloidal systems. Stable nanosilver suspensions are suitable as vehicles for nano-medicine delivery [16], fluorescent sensors [17], and SERS platforms [18].

On the other hand, controlled detachment of the ligand from the nanoparticle surface is required when particle sedimentation is intended, e.g., in water treatment [19], and in conductive ink formulations for printed electronics [20]. Aggregation of PAA-coated AgNPs can be induced by the addition of solvents with a lower dielectric constant than that in which the AgNPs are dispersed, which reduces repulsive interactions. However, from a preparative standpoint this approach requires substantial amounts of organic solvents, which may not result in an environmentally friendly or even cost-effective synthesis. Recently, weak organic or strong mineral acids were also shown to induce aggregation [21,22]. The effect of different ionic species on the aggregation of nanosilver particles has been the subject of several research studies, mainly performed on citrate- and poly(vinylpyrrolidone)-capped AgNPs [23–26]. However, detailed insights into the mechanism of anion-induced aggregation of PAA-AgNPs have never been reported. This is partly due to the complexity of the phenomena occurring at the interface between AgNP and polyacid and buffer, i.e., the impossibility to unambiguously determine the interactions between AgNP and solvent, AgNP and PAA, AgNP and PAA and anions, and PAA-PAA or PAA-solvent interactions solely by

experimental studies alone. Therefore, numerical simulations make an important contribution to the interpretation of these phenomena by providing an in-depth first principles insight into the interactions of the acid-conjugate base with PAA and silver nanoclusters.

Previously published spectroscopic and cyclic voltammetry studies have undeniably shown that the stability of the PAA-AgNPs suspension is disrupted when the same amount of HClO₄ and H₃PO₄ is added. This effect is clearly evidenced by the previously published spectra, which imply that the aggregation of the AgNPs and their current response in the voltammogram is significantly reduced [22]. However, an interesting effect was observed: AgNPs coagulated with HClO₄ and later redispersed exhibited higher anodic current maxima and surface plasmon resonance (SPR) intensity bands as compared to the those coagulated with H₃PO₄. Although perchloric acid is one of the strongest Brønsted-Lowry acids [27], both electrochemical and UV-Vis spectroscopy techniques have clearly shown that the stability of PAA-AgNPs in suspension is affected by the action of HClO₄ to a lesser extent than by equimolar H₃PO₄. Thus, the strength, i.e., the pK_a of the acid appears to be a less relevant factor for the aggregation of AgNPs stabilized with the poly(acrylic acid). This result suggests that the interactions between the weak conjugate base of the acid, AgNP and PAA have a more intricate role and prompted our research to clarify these observations.

2. Materials and methods

2.1. Materials

Silver nitrate (AgNO₃, VWR), hydrazine monohydrate (N₂H₄ × H₂O, 50–60% wt., Sigma Aldrich), poly(acrylic acid) (PAA, M_w = 1800, Sigma Aldrich) were used for the preparation of AgNPs. Sodium tetraborate decahydrate (Na₂B₄O₇ × 10H₂O, Kemika) and boric acid (H₃BO₃, Acros Organics) were used to prepare borax/boric acid (BB) buffer used for spectroscopic characterization. Perchloric (HClO₄, Kemika), phosphoric acid (H₃PO₄, Kemika), sodium perchlorate (NaClO₄, Kemika) and potassium dihydrogenphosphate (KH₂PO₄, Kemika) were used to study the effect of acid addition and acid conjugate base on the stability of PAA coating on AgNPs. pH was adjusted with sodium hydroxide (NaOH, Kemika). D-mannitol (Lach-ner) was used to calibrate the instrumental response of the total organic carbon analyzer. All solutions were prepared with ultrapure water obtained from a GenPure system (TKA, Germany). All the chemicals used in the experiments were of analytical grade (p.a.) purity and were used without additional purification.

2.2. Spectroscopic characterization of the effect of conjugate bases on AgNP dispersions

An aqueous suspension of stabilized silver nanoparticles was prepared by the chemical reduction of the silver(I) precursor. This involved the use of hydrazine hydrate as the reductant and poly(acrylic acid) as a capping agent, according to a previously published procedure [22]. The precipitation step was omitted as to not affect the PAA molecules adsorbed to the surface of AgNPs. Prior to each analysis, the silver nanoparticle suspension was dispersed using a Sonorex Super RK 31 H ultrasonic water bath (Bandelin, Germany) for 5 min to ensure homogeneity. For spectroscopic investigation, 10 μL of the prepared AgNP stock suspension was diluted in a 10 mM sodium tetraborate/boric acid buffer (pH = 8.31). 1 mL of the sample was transferred to a disposable cuvette with an optical path length of 1 cm. To this sample, a pre-calculated amount of either dihydrogenphosphate (H₂PO₄⁻) or perchlorate (ClO₄⁻) containing salts were added in a stepwise concentration, with the initial concentration of the salt being 50 mM and the final being 150 mM. The stock solution concentration for both of these precursors was 0.5 mol dm⁻³, as to minimize the dilution effects on the sample. The absorption spectra of the samples were characterized by a DMS80 UV-Vis spectrophotometer (Varian, USA), using a wavelength range from 700 nm – 350 nm, at a scan rate of 100 nm min⁻¹.

2.3. Characterization of AgNP powders

The effects of H_3PO_4 and HClO_4 , i.e., their respective conjugate bases, on the residual PAA content after precipitation and washing of the precipitate were investigated. Firstly, thermal analysis, i.e., differential scanning calorimetry (DSC) was performed on a DSC 3500 (Netzsch, Germany) calorimeter in the temperature range from 30°C to 300°C at a ramp rate of $20^\circ\text{C min}^{-1}$ under nitrogen atmosphere. Aluminium crucibles with pierced lids were used for this purpose. In addition to DSC, the residual content of PAA was determined by solid sample total organic carbon analysis (SSM-TOC). For that purpose, a TOC-V CPN (Shimadzu, Japan) organic carbon analyzer equipped with a SSM 5000-A solid sample module (Shimadzu, Japan) was used. The combustion was carried at a temperature of 900°C in a pure oxygen atmosphere ($\geq 99.999\%$ O_2), based on available thermogravimetric analyses which imply complete decomposition of PAA occurs at a temperature lower than 800°C [28,29]. D-mannitol was used to prepare the calibration curve ranging from 0.5 to 5 ppm of carbon at 1.5 ppm intervals. The D-mannitol was dried overnight under vacuum at 60°C and weighed in clean ceramic sample boats and covered with a fine ceramic fibre wool. Both sample boat and ceramic fibre wool were calcined beforehand at 950°C for 1 hour in a muffle furnace (LP-07, Instrumentaria) and stored beforehand in a nitrogen-purged desiccator.

The effects of H_3PO_4 and HClO_4 on the crystal structure of the AgNPs was characterized using an XRD-6000 (Shimadzu, Japan) diffractometer. The XRD was equipped with an X-ray copper target tube ($K\alpha$ 1.5406 Å), operated at 40 kV and 30 mA. The diffraction patterns were recorded in the 2θ range from 30° to 85° at a step size of 0.02° and exposure of 2 s. The line shape and position of the diffractometer were calibrated beforehand using an SRM 640e silicon powder standard (Sigma Aldrich, USA). The lattice cell parameters of AgNPs were obtained by Rietveld refinement using DIFFRAC.TOPAS v5.0 (Bruker, USA). The obtained diffraction patterns were compared with reference data available in the Crystallography Open Database (COD). The structural parameters of silver, given by Novgorodov et al. [30] have been used as the initial values in the refinements. The goodness of fit was evaluated by the profile R -factor (R_{wp}) and the expected R -factor (R_{exp}), with results $R_{\text{wp}} < 5\%$ and $R_{\text{exp}} < 3\%$ were considered as satisfactory.

2.4. Computational details

Density functional theory (DFT) was used to investigate the interactions between H_2PO_4^- , ClO_4^- and model AgNPs with $n(\text{Ag}) = 4, 6, 8, 10, 12$ and 14 . For that purpose, geometry optimizations with the Bery algorithm as implemented in Gaussian16 rev.C01 were performed [31]. The calculations have been carried out with the pure PBE correlation-exchange and the hybrid M06-2X hybrid functionals to assure the robustness of the results, whereas the Stevens-Basch-Krauss-Jansien-Cundari (SBKJC) effective core potential basis set modified by adding one f gaussian type function to better describe the polarization of the Ag atoms. For the rest of the atomic centers the 6-311+G** basis set was chosen [32–36]. The SBKJC basis set was chosen on the basis of calculations on Au clusters reported in literature [37], which suggest a good ratio between accuracy and computational cost. In all cases non-covalent interactions have been addressed by using the widely applied and tested Grimme's empirical dispersion [38] during all geometry optimization computations. Furthermore, the counterpoise technique was used to annihilate possible basis set superposition errors in the computation of complexation energies. Default Gaussian16 convergence criteria were used for the geometry optimization. In addition, a superfine integration grid with an accuracy of the two-electron integrals and derivatives set to 10^{-13} Ha was utilized. Further computational investigations entailed the interactions of the Ag_{14} cluster with PAA, PAA- H_2PO_4^- and PAA- ClO_4^- . The model PAA was partially deprotonated ($\text{C}_{12}\text{H}_{16}\text{O}_8^{2-}$), in order to emulate the acid-base equilibrium of PAA occurring under experimental aqueous

conditions. These calculations were performed with the PBE correlation-exchange functional using the previously described basis set, except for computations of charge decomposition analysis (CDA) where the 6-311 G** basis set was employed for the ligands. The CDA analysis was carried out in Multiwfn 3.8.[39], the projected density of states (PDOS) analysis of the molecular orbital occupancy was performed by GaussSum 3.0 [40] and the root mean square distance (RMSD) comparison of the silver clusters was done in Chemcraft 1.8.

3. Results and discussion

3.1. Spectroscopic and thermal characterization of acid-induced aggregation of PAA-capped AgNPs

The addition of organic or mineral acids into the suspension of PAA-capped AgNPs firstly leads to the protonation of the free, i.e., non-AgNP bonded carboxyl groups of PAA according to Eq. (2):



Progressive protonation of PAA leads to a decrease in the extent of electrostatic stabilization of the capped AgNPs. At pH 8, the degree of ionization of PAA is approximately 56%, at pH 6 equals 16% and at pH 4 is less than 5% [41], thus indicating that at acidic pH steric stabilization is the sole contributor to dispersion stability. Not only does protonation lead to the weakening of the electrostatic stabilization, but may cause conformational changes of PAA as well. Large molecular weight PAA ($M_n > 16.5$ kDa) undergoes a conformational change in acidic medium, called hypercoiling, in which individual macromolecules form globules. Hypercoiling of large PAA molecules over AgNPs provides effective steric stabilization, as demonstrated by molecular dynamics studies of AgNP-PAA systems [42]. In such cases, a sufficiently large globule of PAA in which an AgNP is embedded may provide sufficient stabilization and protection from chemical reactions with solutes. In the case of smaller molecular weight PAA as capping agents, hypercoiling does not occur, however it is hypothesized that numerous PAA form an adsorbed monolayer on AgNPs, and stick out towards the bulk solution, providing much needed steric stabilization to prevent aggregation and agglomeration. Studies on the formation of self-organized monolayers (SAMs) of alkyl carboxylic acids on silver have shown that carboxylic acids bind dissociatively onto silver surfaces [43,44]. Hence, protonated PAA has a lower affinity towards adsorption on silver, which promotes its displacement by other species. According to gas phase interaction studies, the desorption energies of alkyl carboxylic acid steadily increase with increasing alkyl chain length. More specifically, the adsorption energy equals $10.6 + 0.9n$ kcal mol $^{-1}$ [45], where n equals the number of $-\text{CH}_2-$ units, which implies greater affinity of longer chain alkyl carboxylic acids towards silver. This opens the possibility if the capping agent monolayer is not tightly packed onto the AgNP surface, solutes such as weak conjugate bases, may interact with PAA-AgNP interface and lead to the displacement of the capping agent.

To assess the effect of the weak conjugate base on the PAA capping layer, dilute aqueous H_3PO_4 and HClO_4 solutions were added to AgNP dispersions in a controlled fashion until an identical pH endpoint was achieved (pH 2.0). After drying of the washed precipitates, and thorough homogenization by pestle and mortar, the samples were analyzed by thermal methods. The thermograms of AgNPs precipitated with 0.01 M H_3PO_4 and HClO_4 , Fig. 1 (A) and 0.1 M H_3PO_4 and HClO_4 , Fig. 1 (B), show two distinct exothermic peaks in all cases, which can be attributed to the decomposition of PAA. More specifically, the peak occurring at a lower temperature, in the interval from 150°C to 210°C , indicates decarboxylation of PAA, whereas the peak at a higher temperature interval, 210°C to 270°C , indicates chain scission of the carbonaceous residue [46]. The decomposition temperature of PAA adsorbed to AgNPs is lower in relation to pristine PAA, indicating catalytic activity of AgNPs towards thermolysis of PAA [46]. The calorimetric enthalpy (ΔH_{cal})

obtained for H_3PO_4 is greater than for HClO_4 in both cases of acid concentration, as shown in Table 1. DSC analysis revealed that i) a relatively larger amount of PAA remains adsorbed on AgNPs when precipitated with H_3PO_4 in relation to HClO_4 , ii) the relative adsorbed amount of PAA is strongly dependent on the concentration of the acid added, i.e., dilution of the AgNP suspension. In order to test the first hypothesis, the samples precipitated with 0.10 M acids were submitted to solid TOC analysis. SSM-TOC analysis confirmed that a relatively larger amount of PAA was adsorbed on AgNPs when precipitated with H_3PO_4 . More specifically, for the AgNPs precipitated with 0.10 M H_3PO_4 the TOC was 0.011 mg(C)/mg, whereas for the 0.10 M HClO_4 the TOC was 0.008 mg(C)/mg, reasonably reflecting the relative ratios of the calorimetric enthalpies from Table 1.

In addition to DSC and SSM-TOC analyses, we have performed thermogravimetric analysis (TGA), for which details are provided in the Supplementary Information (S1.1.). The thermograms presented in Figure S2 reveal subtle, but discernible differences in the thermal behaviours of AgNPs precipitated using HClO_4 and H_3PO_4 at 0.01 M and 0.1 M concentrations, respectively. These thermograms indicate that

Table 1

Calorimetric enthalpies (ΔH_{cal}) and midpoint temperatures (T_{mid}) for the exotherms shown on Fig. 1 DSC thermograms of AgNPs precipitated with H_3PO_4 and HClO_4 :

acid	c, mol dm ⁻³	temperature interval 150 °C – 210 °C		temperature interval 210 °C – 270 °C	
		ΔH_{cal} , J g ⁻¹	T_{mid} , °C	ΔH_{cal} , J g ⁻¹	T_{mid} , °C
H_3PO_4	0.01	-3.52	186.6	-3.35	243.2
	0.10	-1.41	190.4	-2.42	249.0
HClO_4	0.01	-2.26	189.0	-3.46	244.3
	0.10	-0.61	191.1	-1.86	246.1

PAA-capped AgNPs precipitated with HClO_4 exhibit a lesser degree of mass loss compared to the ones precipitated with H_3PO_4 , indicating that a relatively greater amount of PAA was removed by HClO_4 . In addition, the higher concentrations of both of the acids result in a lower mass loss, i.e., less PAA remains on the AgNPs. This suggests that HClO_4 is more effective in removing PAA from the AgNPs. Initially, the sample mass exhibits a slight mass increase, ranging from 0.03% to 0.06%, within the

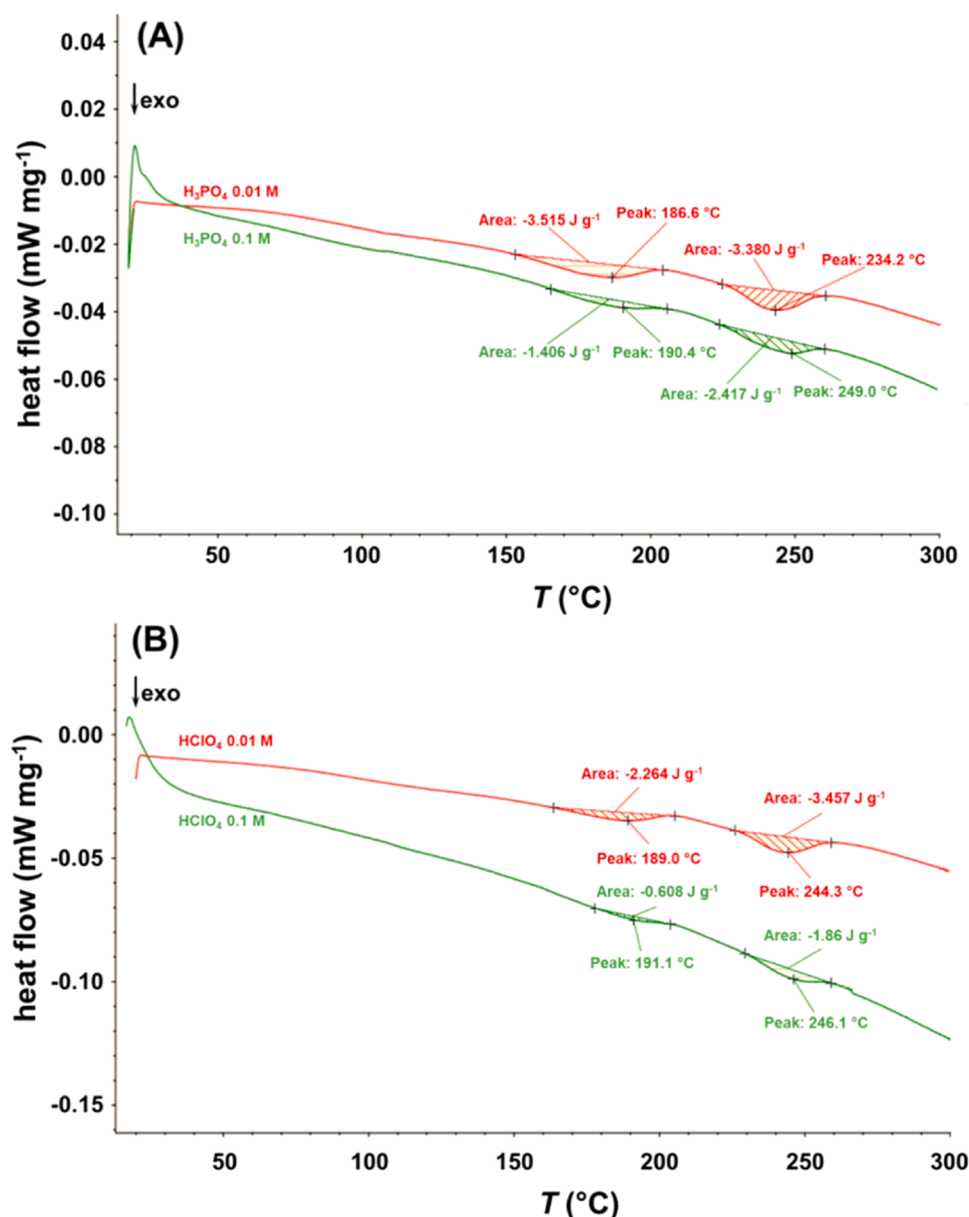


Fig. 1. Heat flow of PAA-capped AgNPs precipitated with 0.01 M H_3PO_4 and 0.01 M HClO_4 (A) and 0.1 M H_3PO_4 and 0.01 M HClO_4 (B).

temperature range from 105 °C up to 180 °C. This miniscule mass increase is attributable to the entrapment of nitrogen within the melting PAA layer enveloping the silver nanoparticles. Subsequently, degradation of PAA commences by pyrolysis, leading to a net mass reduction. At the 850 °C endpoint, the sample precipitated with 0.1 M HClO₄ has lost just 1.26% of its initial mass, whereas the sample precipitated with 0.1 M H₃PO₄ has lost 2.07%.

Considering previously published dynamic light scattering (DLS) measurements and spectroscopic studies of such AgNPs [22], the findings herein paint a contrasting picture. At first glance, if more PAA remain adhered on the AgNP surface, as determined by DSC, SSM-TOC and TGA, than the hydrodynamic radii should be larger. Such a result was indeed reported for H₃PO₄, where the hydrodynamic radii were on average larger by 7 nm than for the HClO₄ equivalent. However, previously published spectroscopic and cyclic voltammetry studies have shown that for the same quantity of H₃PO₄ added, less PAA remains as a capping agent, since the UV/Vis spectra clearly indicate aggregation of AgNPs upon redispersion. More specifically, the surface plasmon resonance (SPR) in the case of PAA-stabilized silver nanoparticles for sphere-like AgNPs with a diameter less than 10 nm should be observed as an intense band at ~420 nm [47]. Even more so the intensity of the plasmon resonance of H₃PO₄ precipitated AgNPs is lower than for HClO₄. Thus, the strength, i.e., pK_a of the acid is seemingly a less contributing factor and the interactions occurring between the weak conjugated base, AgNP and PAA play a more important role.

3.2. Influence of perchlorate and monophosphate on the acid-induced aggregation of PAA-AgNPs

Buffering silver nanoparticle suspensions to maintain a constant pH during experiments is of necessary to prevent side acid-base reactions that occur due to changes in the pH of the system of interest. Therefore, to study the effects of a monovalent-anion on the stability of a colloidal silver solution, a boric acid-borate buffer system was chosen for several reasons. First, it proved to be a suitable medium for keeping the pH nearly constant during the reactions. Second, there are no the external phosphate influences, as is the case with Britton-Robinson, or simple phosphate buffer [48]. Third, in a slightly alkaline medium (pH = 8.31) the primary buffering species are tetraborate (B₄O₇²⁻) and monohydrogen tetraborate (HB₄O₇) Brønsted bases, thus the borate buffer should not affect the perchlorate or monophosphate species. Thus, the stepwise addition of the HClO₄ and H₃PO₄ salts in a buffered solution will show the direct contribution of their respective weak conjugate bases on the stability of the PAA capping layer. The colloidal stability of PAA-AgNP was monitored by observing changes in surface plasmon resonance bands. The SPR absorbance is a sensitive parameter which directly reflects the physico-chemical changes of the colloidal system. Thus, a shift in the peak position indicates the change of particle hydrodynamic radii, while the decrement in the absolute absorbance value is indicative of loss in the number concentration of stable PAA-AgNPs via oxidation or agglomeration mechanism [49]. The UV-Vis absorption spectra of the prepared AgNP suspensions, Figure S1, exhibited a prominent absorption peak at a wavelength of 417 nm, which is consistent with the previously reported location of surface plasmon resonance (SPR) of such stabilized AgNPs [47]. Regardless of the degree of dilution of the AgNP suspension, the peak wavelength remained unchanged. Furthermore, all presented curves retained a symmetrical shape upon dilution, indicating a narrow particle-size distribution. Fig. 2 (A) shows the resulting SPR spectra after the addition of H₂PO₄⁻ to the AgNPs dispersed in the BB buffer, whereas Fig. 2 (B) shows the SPR spectra after ClO₄⁻ addition. The initial addition of H₂PO₄⁻ resulted in a less notable change in the SPR intensity over ClO₄⁻, however, at a certain addition the change in intensity is more abrupt for H₂PO₄⁻.

In addition, ClO₄⁻ tends to form aggregates at lower concentrations, as indicated by the formation of tailing at longer wavelengths (above 500 nm) for a wider range of concentrations. Therefore, ClO₄⁻ will more

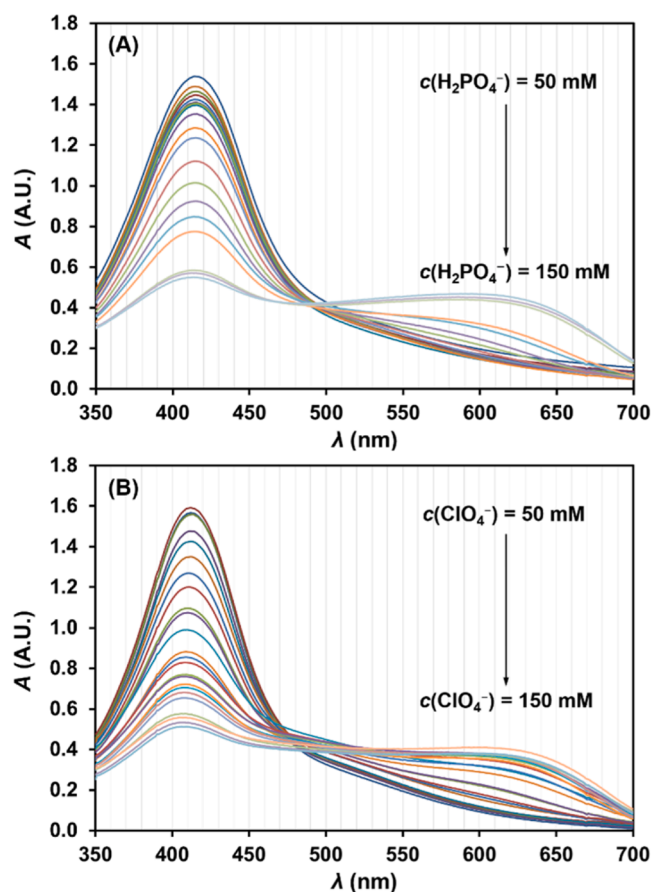


Fig. 2. SPR bands of AgNPs in borax/boric acid buffer solution (pH = 8.31) upon addition of KH₂PO₄ (A) and NaClO₄ (B) in the range of concentration from 50 mM to 150 mM.

effectively displace PAA from the surface of AgNPs at the same pH. Considering that ClO₄⁻ is an oxidizing agent, albeit a weak one at the studied pH, partial oxidation of AgNPs may occur. Upon the addition of ClO₄⁻, a blue-shift of the SPR bands was observed as can be seen on Fig. 2 (B). The blue-shift of the SPR bands in the case of AgNPs is caused by electron spill-out and screening from the *d*-electrons [50] due to the electron accepting nature of ClO₄⁻. Oxidative dissolution of AgNPs, i.e., the release of ionic silver from AgNPs by hydrogen peroxide, hypochlorous acid, and chlorine is well documented [51–53]. However, cyclic voltammograms from a previous study [22] revealed that no ionic silver could be detected after addition of HClO₄ to PAA-AgNPs as evidenced by the decreasing peak oxidative current with the addition of HClO₄ during positive polarization, concurrent with the decrease of the SPR band amplitude. Thus, if oxidation is occurring, it would be mostly limited to the formation of partially oxidized silver species which would protect further dissolution of AgNPs, akin to the study of the effect of hypochlorite on AgNPs by Molleman et al. [54]. The SPR spectra in Fig. 2 (B) support this hypothesis, as a gradual shift to lower wavelengths is noticeable upon addition of further ClO₄⁻, which can be attributed to a decrease of electron density in the silver clusters by the electron-withdrawing oxygen functional moiety and detachment of PAA from the surface by negative electrostatic interactions.

Further insight into the intricacies of the interactions can be obtained from SPR bands by spectroscopic titration of the samples. Spectroscopic titration has shown that two sigmoidal transitions of the SPR at λ = 417 nm can be observed when KH₂PO₄ is added, Fig. 3(A), whereas singular sigmoidal response, Fig. 3(B), was observed after the addition NaClO₄. For the investigated system, the first inflection point for the addition of H₂PO₄⁻ corresponds to the addition of 73 mM of KH₂PO₄,

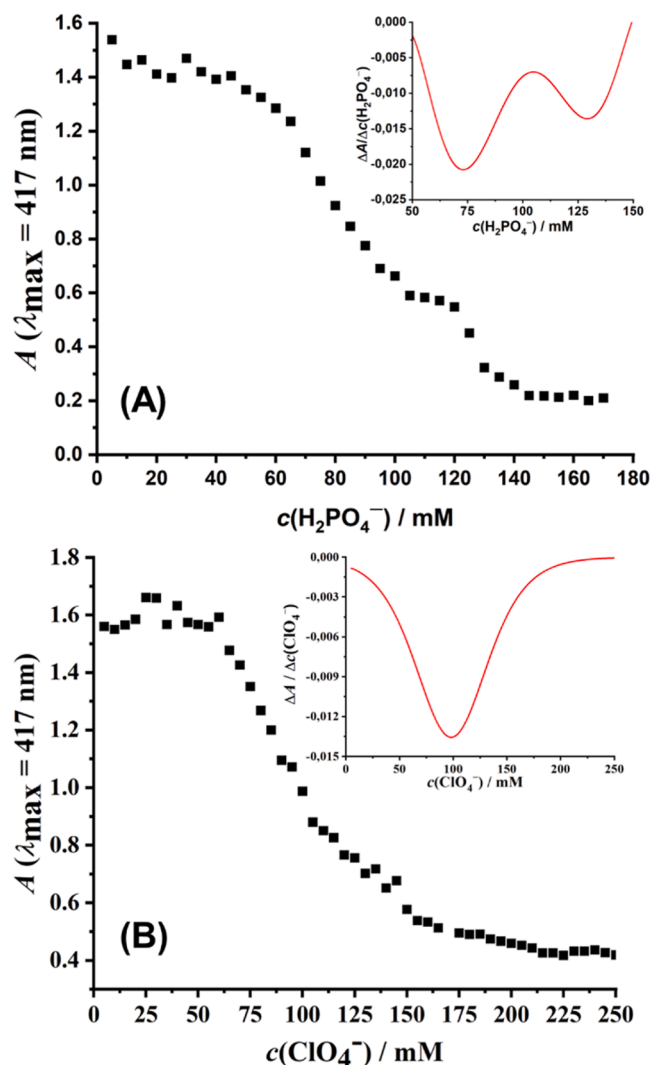


Fig. 3. Spectroscopic titration curves of PAA-AgNPs in borate buffer (pH = 8.31), with inserted graphs denote first derivations of the corresponding fitted functions, for the addition of (A) KH_2PO_4 and (B) NaClO_4 .

whereas the second inflection point occurs after the addition of 130 mM of KH_2PO_4 , at which point the SPR bands show significant aggregation, Fig. 2(A).

In the case of the Fig. 3(B) the equivalence point was reached after the addition of 98 mM NaClO_4 . The sigmoidal curves cannot be attributed to acid-base reactions between H_2PO_4^- and PAA, not only due to the fact that the addition was performed in a buffer, but also considering the relative strengths of the acid-base pairs. Considering that the pK_a of H_2PO_4^- is equal to 7.2, while the pK_a of free or surface-bonded PAA is in the region from 4.5 to 6.7 [21,55], depending on molecular mass and attachment to AgNPs, it can be concluded that PAA is a stronger acid than the conjugate base of H_3PO_4 and therefore is not protonated by H_2PO_4^- . However, H_2PO_4^- and HPO_4^{2-} , unlike ClO_4^- , can form hydrogen bonds with deprotonated PAA at the given pH. At the first endpoint H_2PO_4^- effectively displaces PAA from the surface of AgNPs due to its strong chemical affinity for silver. The chemisorbed $\text{H}_2\text{PO}_4^-/\text{HPO}_4^-$ on AgNPs then forms a hydrogen bond with PAA, however PAA is not tightly bound to the surface of AgNPs anymore. At the second equivalence point, the growing concentration of $\text{H}_2\text{PO}_4^-/\text{HPO}_4^-$ has led to the formation of numerous $\text{H}_2\text{PO}_4^-/\text{HPO}_4^-$ - PAA hydrogen bonds, either between $\text{H}_2\text{PO}_4^-/\text{HPO}_4^-$ in solution and those chemisorbed on considerably decapped AgNPs. The decapped AgNPs then aggregate, which is presumably mediated by the chemisorbed phosphate species.

3.3. Interaction insights at the atomic level

3.3.1. Interactions between silver clusters and H_2PO_4^- , ClO_4^-

To study the interactions of bare silver-nanoclusters with conjugate bases of the chosen mineral acids, geometric optimizations of $\text{Ag}_n\text{-H}_2\text{PO}_4^-$ and $\text{Ag}_n\text{-ClO}_4^-$ complexes were performed at the PBE-D3 and M06-2X-D3 theory levels. Ag_n clusters were optimized accordingly beforehand, a brief discussion is provided within the [Supplementary materials, Section 1.2](#). Computed complexation energies affected by the basis set superposition error have been treated by the widely applied counterpoise method [56,57] and were found to be negative, indicating favourable interactions, consistent with chemical intuition. The trend of corrected complexation energies of the $\text{Ag}_n\text{-H}_2\text{PO}_4^-$ determined by PBE-D3 are shown on Fig. 4(A) and $\text{Ag}_n\text{-ClO}_4^-$ complexes determined by M06-2X-D3 are shown on Fig. 4(B). Frequency analyses revealed that the obtained vibrations of the complexes are real in all cases, thus the optimized geometries should represent true minima of the corresponding potential energy surfaces. The complexation energy in the order of $-23.7 \text{ kcal mol}^{-1}$ to $-53.3 \text{ kcal mol}^{-1}$ indicate bond formation between AgNPs and ClO_4^- and H_2PO_4^- . The obtained results with the PBE-D3 functional are in accord with the more accurate, but more computational demanding hybrid M06-2X functional [58].

For the sake of brevity, only the interactions with Ag_{14} silver clusters will be discussed further, a more detailed discussion on the interactions of individual clusters is provided in the [Supplementary material, Section S1.3](#). Furthermore, the Ag_{14} clusters have both electron-rich and electron-deficient fringes in relation to other clusters, as can be seen from [Figure S6](#) and [Figure S7](#), thus it can serve as a good representative example of attractive and/or repulsive interactions with the ions of interest.

The computed silver to dihydrogenphosphate interatomic distances ($\text{Ag}_{14}\text{-O-PO}_5$) of 2.31 Å to 2.36 Å are remarkably similar regardless of the theory level. In addition, they are in reasonable agreement with the experimentally determined interatomic distance for Ag_2HPO_4 crystal [59]. The same trend holds in the case of $\text{Ag}_{14}\text{-O-ClO}_5$. The computed interatomic distances were found to be 2.31 Å at PBE-D3 level whereas the M06-2X-D3 method predicts somewhat larger interatomic distances of about 2.42 Å. The Ag-O interatomic distance obtained and PBE-D3 was similar to the one reported for the optimized structure of an AgClO_4 crystal by periodic calculations using plane-wave basis sets at the LDA level of theory [60]. Thus, PBE-D3 can be deemed to provide reasonable complexation energies and interatomic distances which are in good agreement with M06-2X-D3 and literature.

In a further step, the nature of the bonding between the conjugated acid bases and Ag_{14} clusters at the PBE-D3 and M06-2X-D3 level was investigated using the charge decomposition analysis (CDA) [61,62]. The CDA approach treats the Kohn-Sham molecular orbitals (MOs) as linear combinations of the electron donor and acceptor MOs, decomposing them the interaction into three terms, namely: (i) donation of electrons (d) from the occupied MOs of the donors to the unoccupied MOs of the acceptor, including the effect of charge reorganization, polarization, exchange and charge transfer, (ii) back-donation (b) which includes the interaction between the occupied MOs of the acceptor and the unoccupied MOs of the donor, as well as (iii) repulsive polarization (r). Thus, conjugated acids can be considered as electron donors and the silver cluster as acceptor. The results of the CDA analysis are shown in [Table 2](#).

Calculations according with either functional indicate charge transfer to the empty orbitals of Ag_{14} from both H_2PO_4^- and ClO_4^- via σ -donation, as depicted by the orbitals with the largest donor parameter in [Fig. 5](#). Thus, either H_2PO_4^- and ClO_4^- should form dative bonds with the atoms of the silver clusters. The tendency of the cluster considered in this analysis is to accept electrons as a result of relative electron deficiency spotted on the fringe atoms of the cluster. The isovalue orbital lobe density in conjunction with complexation energies, along with the CDA analysis results in [Table 2](#), imply that the π orbitals of H_2PO_4^- are

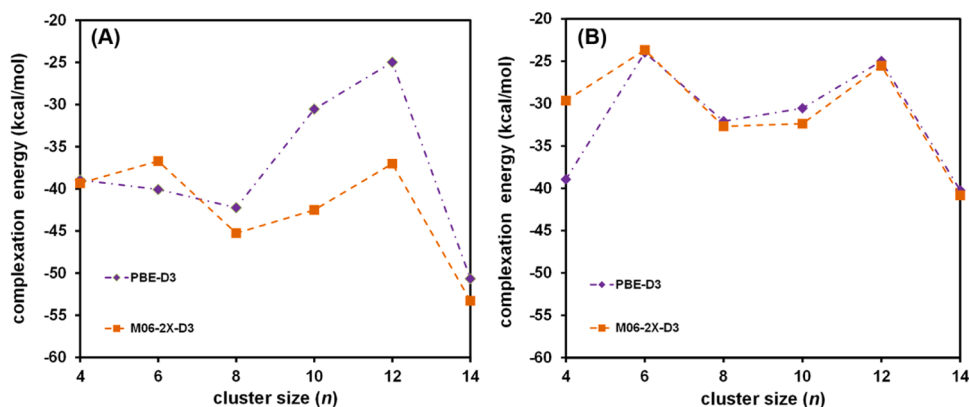


Fig. 4. Basis set superposition error corrected complexation energies of the (A) $\text{Ag}_n\text{-H}_2\text{PO}_4^-$ and (B) $\text{Ag}_n\text{-ClO}_4^-$ complexes determined by PBE-D3 and M06-2X levels of theory.

Table 2

CDA analysis of $\text{Ag}_{14}\text{-H}_2\text{PO}_4^-$ and $\text{Ag}_{14}\text{-ClO}_4^-$ complexes, in which Ag_{14} is the acceptor and conjugated bases are electron donors.

functional	$\text{Ag}_{14}\text{-H}_2\text{PO}_4^-$			$\text{Ag}_{14}\text{-ClO}_4^-$		
	<i>d</i>	<i>b</i>	<i>r</i>	<i>d</i>	<i>b</i>	<i>r</i>
PBE-D3	0.363	<0.01	-0.295	0.223	<0.01	-0.235
M06-2X-D3	0.280	<0.01	-0.238	0.186	<0.01	-0.238

able to form stronger σ bonds with the silver cluster than ClO_4^- . The extent of π -backdonation (*b*) from Ag_{14} , which in general contributes significantly to the stability of the complex, is negligible. The π -backdonation is hindered by the unfavourable energy levels of the occupied MOs of Ag_{14} and the unoccupied MOs of the conjugated acids, i.e., the HOMO of Ag_{14} in the complex has a significantly lower energy than the LUMO of the two conjugated acids. The HOMO of the complexes is of a higher energy than the HOMO of the single Ag_{14} cluster, i.e., the HOMO of the Ag_{14} cluster alone is -4.371 eV, whereas the HOMO of the $\text{Ag}_{14}\text{-H}_2\text{PO}_4^-$ is at -1.328 eV. Based on the approach by Zhan et al. [63], the energies of HOMOs in DFT calculations provides an indication of the

corresponding ionization potential. Thus, the bond formed in $\text{Ag}_{14}\text{-H}_2\text{PO}_4^-$ complex should be relatively weak. The natural electron configuration of the electron deficient atoms can be described as $5s^{0.66}4d^{9.98}5p^{0.05}$ at the M06-2X level on the other hand the more electron rich atoms in the Ag_{14} cluster the electron configurations are described as $5s^{0.50}4d^{9.97}5p^{0.90}$ at the same level of theory. Thus, the donated electrons should not concern 4d silver orbitals, which are highly localized [64].

As can be seen from the MO density on Fig. 5(A) and 5(B), the charge transfer from H_2PO_4^- results in significant charge delocalization within the interacting silver cluster. The dipole moments of the complexes, shown in Table S3, reveal that the AgNPs interacting with ClO_4^- should be more polarized than those with H_2PO_4^- . NBO analysis was performed to elucidate the electron configuration of the atoms in the clusters. The formation of the $\text{Ag}_{14}\text{-H}_2\text{PO}_4^-$ bond resulted in partial filling of the electron deficient cluster, in which the populations of the occupied valence shell in the case of M06-2X are described as $5s^{0.45}4d^{9.95}5p^{0.28}$. In brief, NBO analysis has revealed that the Ag_{14} cluster received 0.23 electrons at the M06-2X-D3 level. The obtained results with the M06-2X functional are found to be close to the computations obtained

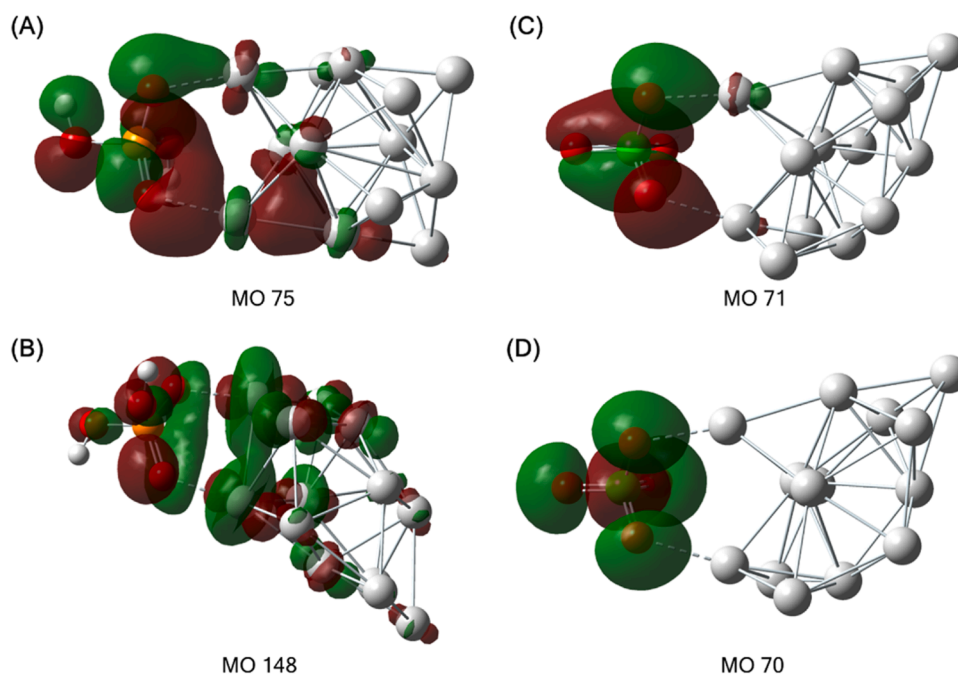


Fig. 5. Molecular orbitals (MOs, isovalue 0.02 a.u.) with the largest electron donating contributions to the Ag_{14} cluster from H_2PO_4^- determined by (A) PBE-D3 and (B) M06-2X-D3; and of ClO_4^- to Ag_{14} determined by (C) PBE-D3, (D) M06-2X-D3.

with the less expensive in terms of computing time PBE-D3, thus, hereafter all further discussion will be based solely on the PBE-D3 approach [38].

3.3.2. Interaction of silver clusters with PAA

Favourable interactions of the carbonyl groups of PAA and polyelectrolytes in general with silver at the surface of the nanoparticles are known to yield effective stabilization of AgNPs in dispersion. There seems to be a broad consensus that the interaction of AgNPs and PAA can be described as an adsorption process that leads to the formation of a monolayer on the surface of AgNPs. However, an aspect often overlooked is that PAA is able to provide effective stabilization even at exceedingly low ratios of $n(\text{Ag}): n(\text{PAA}) = 1 \times 10^{-3} \text{ mol dm}^{-3}: 5 \times 10^{-10} \text{ mol dm}^{-3}$ [65]. Such a low ratio may imply that the surface of AgNPs is saturated with PAA well before a monolayer is formed, hence further addition of PAA to the system does not provide much benefit as it remains in solution. For reference, the molar ratio of $n(\text{Ag}): n(\text{PAA})$ herein corresponds to 0.06, whereby the concentration of PAA was $0.062 \text{ mol mol dm}^{-3}$ [47], i.e., well in excess of the minimum ratio reported in literature. Kyrychenko et al. [42] have provided some insights into the interactions between PAA with AgNPs in water using the molecular dynamics approach. The aforementioned study has shown that protonated PAA has a tendency to provide a densely packed sheath over the AgNP, with the protonated carboxyl groups oriented towards the surface of the AgNP, leading even to the displacement of water from the interface. However, such a model approach has overlooked the interactions of the deprotonated carboxyl group with the AgNP surface. Having in mind the results shown above, the interactions of the deprotonated carboxyl group are expected to be much stronger, as it is more conducive to charge transfer. One of the aims of this study is to remove the veil of mystery over the AgNP-PAA interactions, and address the problem with DFT. For this purpose, calculations at the PBE-D3/6-311++G(d,p) level were performed revealing that, akin to H_2PO_4^- and ClO_4^- , a donor type orbital is formed between the $-\text{COO}^-$ group of PAA and silver. The counterpoise corrected complexation energy of the $\text{Ag}_{14}\text{-PAA}^-$ is $-67.90 \text{ kcal mol}^{-1}$, indicating strong bonding on AgNPs. In addition, reflecting the greater complexation energy the interatomic distances between the oxygen atoms in the carboxyl group and silver atoms are somewhat shorter than in the case of ClO_4^- and H_2PO_4^- , and for the optimized geometry correspond to 2.25 Å and 2.26 Å, as depicted on Fig. 6(A). Furthermore, electrostatic mapping of the ionized model PAA molecule reveals a strong density of the negative charge on the non-interacting deprotonated carboxyl groups, which would reflect to effective electrostatic stabilization from other ionized

PAA molecules. However, the contribution of the electrostatic stabilization in the vicinity of the Ag_{14} cluster is diminished due to the donation of the electrons from the deprotonated carboxyl group to the cluster. The CDA analysis has revealed that the model PAA molecule donates electrons to a greater extent than either ClO_4^- and H_2PO_4^- , a total of 0.391 electrons, whereby the MOs of the complex with the largest electron donating character are depicted on Fig. 6(B).

3.3.3. Interactions of H_2PO_4^- and ClO_4^- with the Ag_{14} -PAA complex

The study of the interactions between the Ag_{14} cluster and individual H_2PO_4^- , ClO_4^- and PAA has revealed that the complexation is governed by the cluster's affinity towards electrons. Chemical intuition implies that the bulkiness of PAA, coupled with inter- and intra-macromolecular repulsions between ionized carboxyl groups, could greatly limit the extent of the valence shell saturation of the individual clusters by PAA alone. Hence, smaller electron donating species, which can more easily migrate to the surface of the AgNPs, such as H_2PO_4^- and ClO_4^- could satiate the AgNP and cause detachment of PAA. Albeit the model system is very small, the electron affinity of Ag clusters remains relatively unchanged in even-atom clusters from Ag_{14} to Ag_{22} [66], hence the model may act reasonably.

Thus, geometry optimization and calculations described previously were done for the complexes $\text{Ag}_{14}\text{-H}_2\text{PO}_4^-$ -PAA and $\text{Ag}_{14}\text{-ClO}_4^-$ -PAA. The geometries of the optimized complexes are shown on Fig. 7.

As can be seen, the interatomic Ag-O interatomic distances have increased in relation to the values shown above for both $\text{Ag}_{14}\text{-H}_2\text{PO}_4^-$ and $\text{Ag}_{14}\text{-ClO}_4^-$. It is notable that the Ag_{14} clusters in the complexes are severely distorted, i.e., the root mean square distance (RMSD) in comparison to the undistorted cluster is 1.322 Å in the case of $\text{Ag}_{14}\text{-H}_2\text{PO}_4^-$ -PAA, whereas for $\text{Ag}_{14}\text{-ClO}_4^-$ -PAA the RMSD is 0.795 Å. In comparison, PAA alone causes a less pronounced distortion of 0.453 Å. As to be expected, the silver clusters have become significantly more negatively charged in relation to the Ag_{14} -PAA complex shown on Fig. 7(A), even more so in the case of $\text{Ag}_{14}\text{-ClO}_4^-$. CDA analysis has revealed that in the $\text{Ag}_{14}\text{-H}_2\text{PO}_4^-$ -PAA complex PAA has donated 0.370 electrons and H_2PO_4^- 0.240 electrons to the silver cluster. In addition, limited charge transfer occurs between H_2PO_4^- -PAA, whereby PAA donates 0.058 electrons to H_2PO_4^- and H_2PO_4^- backdonates 0.024 electrons. In the $\text{Ag}_{14}\text{-ClO}_4^-$ -PAA complex PAA donates 0.316 electrons to the Ag_{14} cluster, whereas Ag_{14} donates 0.159 electrons to ClO_4^- . Since the negative charge is localized in ClO_4^- , and due to oxidizing nature of perchlorate, the electron density is withdrawn from the now electron rich silver cluster. Unsurprisingly, the total dipole moment in the $\text{Ag}_{14}\text{-ClO}_4^-$ -PAA is about 1.6 times stronger than in $\text{Ag}_{14}\text{-H}_2\text{PO}_4^-$ -PAA, as the charge transfer from Ag_{14} to ClO_4^- causes

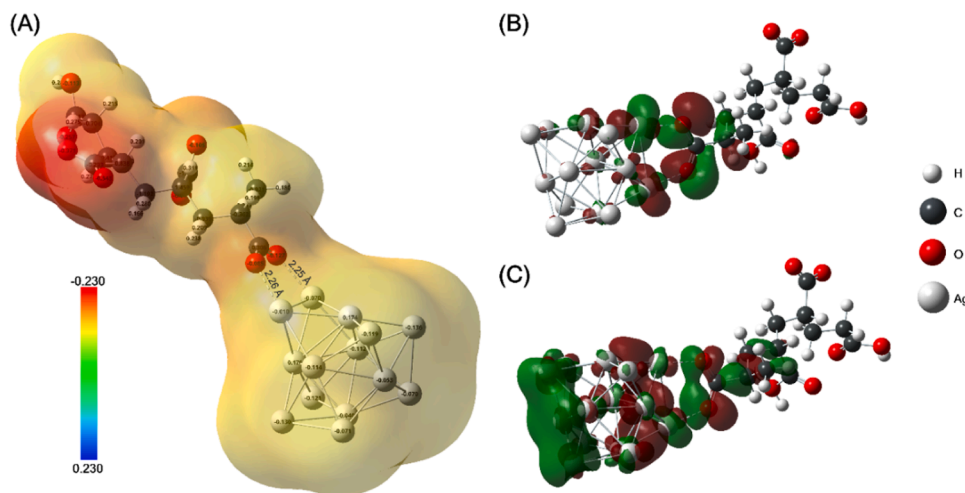


Fig. 6. (A) Molecular electrostatic mapping (ESP) of the complex of Ag_{14} and partially deprotonated PAA ($\alpha = 0.5$), MOs 203 (B) and MO 204 (C) with the largest donor contributions (isovalue 0.02 a.u.).

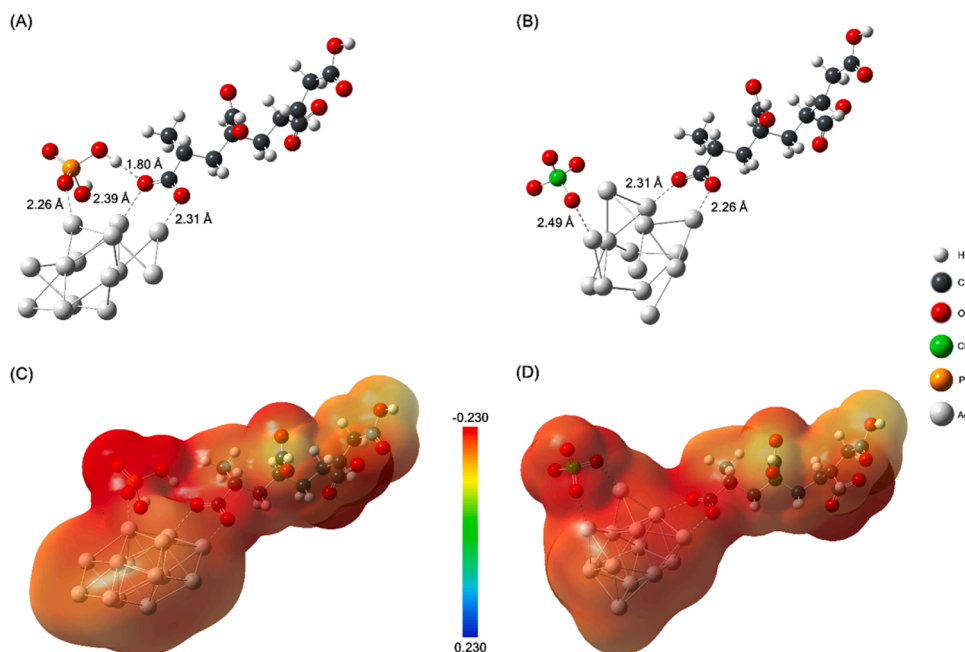


Fig. 7. Optimized geometries of the (A) $\text{Ag}_{14}\text{-H}_2\text{PO}_4\text{-PAA}$ and (B) $\text{Ag}_{14}\text{-ClO}_4\text{-PAA}$ complexes obtained at the PBE-D3 theory level, along with their respective molecular ESP maps for the former (C) and for the latter (D).

further polarization. These complexes have favourable counterpoise corrected complexation energies. Specifically, for $\text{Ag}_{14}\text{-H}_2\text{PO}_4\text{-PAA}$ the complexation energy between the three fragments is -33.62 kcal/mol while in the case of the $\text{Ag}_{14}\text{-ClO}_4\text{-PAA}$ cluster the complexation energy amounts to -84.23 kcal/mol. The mechanism of the relative ease at which ClO_4^- destabilizes PAA-capped AgNPs relative to H_2PO_4^- becomes much more apparent in the light of the results provided by our theoretical calculations. First, ClO_4^- behaves as an opportunistic electron acceptor when PAA donates electrons to the Ag cluster. In such a way, the Ag-PAA donating bond is weakened, as the electrons are distributed away from the Ag-PAA interface. Second, repulsive electrostatic interactions likely occur between ClO_4^- and PAA, leading to eventual detachment of PAA from the surface. H_2PO_4^- , on the other hand, has a significantly lower electron affinity and donates a significant portion of electrons in relation to PAA, which likewise results in a weakening of the Ag-PAA donor bond. In addition, H_2PO_4^- is able to form hydrogen bonds with PAA, thus H_2PO_4^- may cause clumping of individual PAA macromolecules and thereby disrupting steric and electrostatic stabilization. Thus, according to spectroscopic titration on Fig. 3 the first point of equivalence is observed at a lower concentration of H_2PO_4^- than for ClO_4^- . However, further addition of H_2PO_4^- likely leads to the disruption of the hydrogen bonds and thus a second point of inflexion is observed during spectroscopic titration. Finally, the formation of hydrogen bonds may lead to aggregation and consequentially larger hydrodynamic radii, as observed by DLS.

3.4. Effect of the conjugate bases on the structure of AgNPs

The above-mentioned calculations indicate that complexation with H_2PO_4^- , and to a somewhat lesser extent with ClO_4^- distort the structure of the model silver cluster. Although the model silver cluster used in the DFT calculations is sizeably smaller than its real AgNP counterparts, and would therefore exhibit a more pronounced covalent character than AgNPs. Rietveld analysis, Figure S10, on powder X-ray diffraction patterns was performed to elucidate potential distortion of the structure of the real AgNPs. These effects could have practical implications on the reactivity and properties of AgNPs. The diffractograms show that precipitation with either acid results in crystalline AgNPs, with nano-sized

crystallites as indicated by the broad peaks of the silver-specific diffraction planes. In both cases, the AgNPs crystallize in the face-centered cubic structure with space group Fm-3 m. Rietveld analysis of the individual AgNPs revealed that the AgNPs precipitated with H_3PO_4 have a marginally larger crystal cell, with the cell parameter a equal to 4.0898 Å (fit error 0.0026), while for HClO_4 the cell parameter a is equal to 4.0866 Å (fit error 0.0045), resulting in a unit cell volume of 68.4 Å³ for the former and 68.2 Å³ for the latter. Despite these changes in unit cell volume being miniscule, the effects of the conjugated acid bases may be limited only to the near-surface Ag atoms of the AgNPs, Albeit the experimentally determined extent of the distortion of the crystalline structures is much less pronounced in relation to the DFT model system, these results imply that the DFT calculations even on a model system as small as the Ag_{14} cluster, can provide valuable insights into the behaviour of nano-scale systems.

4. Conclusions

Experimental studies on the effect of H_2PO_4^- and ClO_4^- acid conjugate bases have shown that the detachment of PAA from the surface of AgNPs is poorly described by simple acid-base interactions. Spectroscopic titration has indicated that H_2PO_4^- readily forms hydrogen bonds with PAA and that ClO_4^- readily detaches PAA from the surface of AgNPs at lower equivalent concentrations due to its electron accepting nature. Detailed and systematic DFT calculations have revealed that ionized PAA is an effective capping agent for AgNPs as it forms an electron-donor type bond with AgNPs. The weak conjugated acids act as competitive electron donors, leading to the saturation of the AgNP and resulting in a large dipole moment of the complex, polarization of the silver cluster and negative electron affinity. These effects probably result in partial detachment of PAA from the surface of AgNPs and leads to effective precipitation. On the other hand, ClO_4^- acts as a stronger decapping agent due to its electron accepting affinity, leading to effective weakening of the AgNP-PAA donating bond. Nevertheless, H_2PO_4^- can form hydrogen bonds with the carboxyl group of PAA, which is conducive for the aggregation of AgNPs. Finally, the weak mineral conjugated acids distort the clusters somewhat, with H_2PO_4^- resulting in somewhat larger crystallites than ClO_4^- .

CRedit authorship contribution statement

Panaghiotis Karamanis: Writing – original draft, Supervision, Software, Resources, Investigation, Funding acquisition. **Irena Ivanišević:** Writing – original draft, Methodology, Investigation, Formal analysis, Conceptualization. **Antonia Ressler:** Resources, Methodology, Investigation, Formal analysis. **Marin Kovacic:** Writing – original draft, Visualization, Methodology, Investigation, Formal analysis, Data curation, Conceptualization.

Declaration of Competing Interest

The authors declare that they have no known competing financial interests or personal relationships that could have appeared to influence the work reported in this paper.

Data availability

Data will be made available on request.

Acknowledgements

We gratefully acknowledge the Integrated Laboratory for Primary and Secondary Raw Materials (*Integrirani laboratorij za primarne i sekundarne sirovine*) VIRTULAB (KK.01.1.1.02.0022) co-funded by the European Regional Development Fund, on the Faculty of Chemical Engineering and Technology of the University of Zagreb for the DSC measurements. This research was performed using the resources of the computer cluster Isabella based in SRCE – University of Zagreb Computing Centre.

Appendix A. Supporting information

Supplementary data associated with this article can be found in the online version at [doi:10.1016/j.colsurfa.2024.133739](https://doi.org/10.1016/j.colsurfa.2024.133739).

References

- [1] S. Gottardo, A. Mech, J. Drbohlavová, A. Małyska, S. Bówadt, J. Riego Sintes, H. Rauscher, Towards safe and sustainable innovation in nanotechnology: state-of-play for smart nanomaterials, *NanoImpact* 21 (2021), <https://doi.org/10.1016/j.impact.2021.100297>.
- [2] M. Khalil, G.T.M. Kadja, M.M. Ilmi, Advanced nanomaterials for catalysis: current progress in fine chemical synthesis, hydrocarbon processing, and renewable energy, *J. Ind. Eng. Chem.* 93 (2021) 78–100, <https://doi.org/10.1016/j.jiec.2020.09.028>.
- [3] M. Khalil, B.M. Jan, C.W. Tong, M.A. Berawi, Advanced nanomaterials in oil and gas industry: design, application and challenges, *Appl. Energy* 191 (2017) 287–310, <https://doi.org/10.1016/j.apenergy.2017.01.074>.
- [4] M.A. Islam, M.V. Jacob, E. Antunes, A critical review on silver nanoparticles: From synthesis and applications to its mitigation through low-cost adsorption by biochar, *J. Environ. Manag.* 281 (2021) 111918, <https://doi.org/10.1016/j.jenvman.2020.111918>.
- [5] P.M. Potter, J. Navratilova, K.R. Rogers, S.R. Al-Abed, Transformation of silver nanoparticle consumer products during simulated usage and disposal, *Environ. Sci.: Nano* 6 (2) (2019) 592–598, <https://doi.org/10.1039/C8EN00958A>.
- [6] J. Pulit-Prociak, M. Banach, Silver nanoparticles – a material of the future...? *Open Chem.* 14 (1) (2016) 76–91, <https://doi.org/10.1515/chem-2016-0005>.
- [7] Y. Wang, J. He, C. Liu, W.H. Chong, H. Chen, Thermodynamics versus kinetics in nanosynthesis, *Angew. Chem. - Int. Ed.* 54 (7) (2015) 2022–2051, <https://doi.org/10.1002/anie.201402986>.
- [8] N.M. Kovalchuk, V.M. Starov, Aggregation in colloidal suspensions: Effect of colloidal forces and hydrodynamic interactions, *Adv. Colloid Interface Sci.* 179–182 (2012) 99–106, <https://doi.org/10.1016/j.cis.2011.05.009>.
- [9] H. Heinz, C. Pramanik, O. Heinz, Y. Ding, R.K. Mishra, D. Marchon, R.J. Flatt, I. Estrela-Lopis, J. Llop, S. Moya, R.F. Ziolo, Nanoparticle decoration with surfactants: molecular interactions, assembly, and applications, *Surf. Sci. Rep.* 72 (1) (2017) 1–58, <https://doi.org/10.1016/j.surfrep.2017.02.001>.
- [10] V. De Matteis, M. Cascione, C.C. Toma, S. Leporatti, Silver nanoparticles: synthetic routes, in vitro toxicity and theranostic applications for cancer disease, *Nanomaterials* 8 (5) (2018) 319, <https://doi.org/10.3390/nano8050319>.
- [11] I. Ivanišević, S. Milardović, P. Kassal, Recent advances in (bio)chemical sensors for food safety and quality based on silver nanomaterials, *Food Technol. Biotechnol.* 59 (2) (2021) 216–237, <https://doi.org/10.17113/ftb.59.02.21.6912>.
- [12] A. Arya, V. Mishra, T.S. Chundawat, Green synthesis of silver nanoparticles from green algae (*Botryococcus braunii*) and its catalytic behavior for the synthesis of benzimidazoles, *Chem. Data Collect.* 20 (2019) 100190, <https://doi.org/10.1016/j.cdc.2019.100190>.
- [13] I.J. Fernandes, A.F. Aroche, A. Schuck, P. Lamberty, C.R. Peter, W. Hasenkamp, T. L.A.C. Rocha, Silver nanoparticle conductive inks: synthesis, characterization, and fabrication of inkjet-printed flexible electrodes, *Sci. Rep.* 10 (1) (2020) 8878, <https://doi.org/10.1038/s41598-020-65698-3>.
- [14] R.-L. Wang, D.-P. Li, L.-J. Wang, X. Zhang, Z.-Y. Zhou, J.-L. Mu, Z.-M. Su, The preparation of new covalent organic framework embedded with silver nanoparticles and its applications in degradation of organic pollutants from waste water, *Dalton Trans.* 48 (3) (2019) 1051–1059, <https://doi.org/10.1039/C8DT04458A>.
- [15] A. Sadeghpour, A. Vaccaro, S. Rentsch, M. Borkovec, Influence of alkali metal counterions on the charging behavior of poly(acrylic acid), *Polymer* 50 (16) (2009) 3950–3954, <https://doi.org/10.1016/j.polymer.2009.06.032>.
- [16] S.K. Kailasa, M. Chandel, V.N. Mehta, T.J. Park, Influence of ligand chemistry on silver nanoparticles for colorimetric detection of Cr³⁺ and Hg²⁺ ions, *Spectrochim. Acta Part A: Mol. Biomol. Spectrosc.* 195 (2018) 120–127, <https://doi.org/10.1016/j.saa.2018.01.038>.
- [17] L. Burratti, E. Ciotta, E. Bolli, S. Kaciulis, M. Casalboni, F. De Matteis, A. Garzón-Manjón, C. Scheu, R. Pizzoferrato, P. Proposito, Fluorescence enhancement induced by the interaction of silver nanoclusters with lead ions in water, *Colloids Surf. A: Physicochem. Eng. Asp.* 579 (2019) 123634, <https://doi.org/10.1016/j.colsurfa.2019.123634>.
- [18] A.Y. Khrushchev, E.R. Akmaev, A.Y. Gulyaeva, A.V. Zavalov, A.I. Sidorenko, V. O. Bondarenko, A.I. Lvovskiy, Ion-induced agglomeration of Ag NPs for quantitative determination of trace malachite green in natural water by SERS, *Vib. Spectrosc.* 120 (2022) 103360, <https://doi.org/10.1016/j.vibspec.2022.103360>.
- [19] J. Zhao, X. Wang, S.A. Hoang, N.S. Bolan, M.B. Kirkham, J. Liu, X. Xia, Y. Li, Silver nanoparticles in aquatic sediments: occurrence, chemical transformations, toxicity, and analytical methods, *J. Hazard. Mater.* 418 (2021) 126368, <https://doi.org/10.1016/j.jhazmat.2021.126368>.
- [20] I. Ivanišević, P. Kassal, A. Milinković, A. Rogina, S. Milardović, Combined chemical and thermal sintering for high conductivity inkjet-printed silver nanoink on flexible substrates, *Chem. Biochem. Eng. Q.* 33 (3) (2019) 377–384, <https://doi.org/10.15255/CABEQ.2019.1585>.
- [21] I. Ivanišević, V. Rukavina, P. Kassal, S. Milardović, Impact of weak organic acids on precipitation of poly(acrylic acid) stabilized silver nanoparticles; an electrochemical approach, *Croat. Chem. Acta* 91 (4) (2018) 491–499, <https://doi.org/10.5562/cca3445>.
- [22] I. Ivanišević, S. Milardović, P. Kassal, M. Zlatar, Electrochemical and spectroscopic characterization of AgNP suspension stability influenced by strong inorganic acids, *Electrochim. Acta* 377 (2021), <https://doi.org/10.1016/j.electacta.2021.138126>.
- [23] J.M. Gorham, A.B. Rohlffing, K.A. Lipka, R.I. MacCuspie, A. Hemmati, R. David Holbrook, Storage wars: how citrate-capped silver nanoparticle suspensions are affected by not-so-trivial decisions, *J. Nanopart. Res.* 16 (4) (2014), <https://doi.org/10.1007/s11051-014-2339-9>.
- [24] K.A. Huynh, K.L. Chen, Aggregation kinetics of citrate and polyvinylpyrrolidone coated silver nanoparticles in monovalent and divalent electrolyte solutions, *Environ. Sci. Technol.* 45 (13) (2011) 5564–5571, <https://doi.org/10.1021/es200157h>.
- [25] A.M. El Badawy, K.G. Scheckel, M. Suidan, T. Tolaymat, The impact of stabilization mechanism on the aggregation kinetics of silver nanoparticles, *Sci. Total Environ.* 429 (2012) 325–331, <https://doi.org/10.1016/j.scitotenv.2012.03.041>.
- [26] M. Baalousha, Y. Nur, I. Römer, M. Tejamaya, J.R. Lead, Effect of monovalent and divalent cations, anions and fulvic acid on aggregation of citrate-coated silver nanoparticles, *Sci. Total Environ.* 454–455 (2013) 119–131, <https://doi.org/10.1016/j.scitotenv.2013.02.093>.
- [27] J. Zhang, Y. Sun, C. Mao, H. Gao, W. Zhou, Z. Zhou, Theoretical study of pKa for perchloric acid, *J. Mol. Struct.: Theochem.* 906 (1) (2009) 46–49, <https://doi.org/10.1016/j.theochem.2009.03.029>.
- [28] Z. Ni, Z. Wang, L. Sun, B. Li, Y. Zhao, Synthesis of poly acrylic acid modified silver nanoparticles and their antimicrobial activities, *Mater. Sci. Eng.: C.* 41 (2014) 249–254, <https://doi.org/10.1016/j.msec.2014.04.059>.
- [29] P. Chowdhury, A. Hazra, M. Kr. Mondal, B. Roy, D. Roy, S. Prasad Bayen, S. Pal, Facile synthesis of polyacrylate directed silver nanoparticles for pH sensing through naked eye, *J. Macromol. Sci. Part A* 56 (8) (2019) 773–780, <https://doi.org/10.1080/10601325.2019.1607376>.
- [30] M.I. Novgorodovo, A.I. Gorshkov, A.V. Mokhov, Native Silver and Its New Structural Modifications, *Int. Geol. Rev.* 23 (4) (1981) 485–494, <https://doi.org/10.1080/00206818109455083>.
- [31] M.J. Frisch, G.W. Trucks, H.B. Schlegel, G.E. Scuseria, M.A. Robb, J.R. Cheeseman, G. Scalmani, V. Barone, G.A. Petersson, H. Nakatsuji, X. Li, M. Caricato, A.V. Marenich, J. Bloino, B.G. Janesko, R. Gomperts, B. Mennucci, H.P. Hratchian, J.V. Ortiz, A.F. Izmaylov, J.L. Sonnenberg, Williams, F. Ding, F. Lipparini, F. Egidi, J. Goings, B. Peng, A. Petrone, T. Henderson, D. Ranasinghe, V.G. Zakrzewski, J. Gao, N. Rega, G. Zheng, W. Liang, M. Hada, M. Ehara, K. Toyota, R. Fukuda, J. Hasegawa, M. Ishida, T. Nakajima, Y. Honda, O. Kitao, H. Nakai, T. Vreven, K. Throssell, J.A. Montgomery Jr., J.E. Peralta, F. Ogliaro, M.J. Bearpark, J.J. Heyd, E.N. Brothers, K.N. Kudin, V.N. Staroverov, T.A. Keith, R. Kobayashi, J. Normand, K. Raghavachari, A.P. Rendell, J.C. Burant, S.S. Iyengar, J. Tomasi, M. Cossi, J.M. Millam, M. Klene, C. Adamo, R. Cammi, J.W. Ochterski, R.L. Martin, K. Morokuma, O. Farkas, J.B. Foresman, D.J. Fox, *Gaussian 16 Rev. C.01*, Wallingford, CT, 2016.

- [32] R. Krishnan, J.S. Binkley, R. Seeger, J.A. Pople, Self-consistent molecular orbital methods. XX. A basis set for correlated wave functions, *J. Chem. Phys.* 72 (1) (1980) 650–654, <https://doi.org/10.1063/1.438955>.
- [33] J.P. Perdew, K. Burke, M. Ernzerhof, Generalized gradient approximation made simple, *Phys. Rev. Lett.* 77 (18) (1996) 3865–3868, <https://doi.org/10.1103/PhysRevLett.77.3865>.
- [34] Y. Zhao, D.G. Truhlar, The M06 suite of density functionals for main group thermochemistry, thermochemical kinetics, noncovalent interactions, excited states, and transition elements: two new functionals and systematic testing of four M06-class functionals and 12 other functionals, *Theor. Chem. Acc.* 120 (1–3) (2008) 215–241, <https://doi.org/10.1007/s00214-007-0310-x>.
- [35] W.J. Stevens, M. Krauss, H. Basch, P.G. Jasien, Relativistic compact effective potentials and efficient, shared-exponent basis-sets for the third-, fourth-, and fifth-row atoms, *Can. J. Chem. -Rev. Can. De. Chim.* 70 (2) (1992) 612–630, <https://doi.org/10.1139/v92-085>.
- [36] B.P. Pritchard, D. Altaraw, B. Didier, T.D. Gibson, T.L. Windus, New Basis Set Exchange: an open, up-to-date resource for the molecular sciences community, *J. Chem. Inf. Model.* 59 (11) (2019) 4814–4820, <https://doi.org/10.1021/acs.jcim.9b00725>.
- [37] P.K. Jain, A DFT-based study of the low-energy electronic structures and properties of small gold clusters, *Struct. Chem.* 16 (4) (2005) 421–426, <https://doi.org/10.1007/s11224-005-6350-8>.
- [38] S. Grimme, J. Antony, S. Ehrlich, H. Krieg, A consistent and accurate ab initio parametrization of density functional dispersion correction (DFT-D) for the 94 elements H-Pu, *J. Chem. Phys.* 132 (15) (2010) 154104, <https://doi.org/10.1063/1.3382344>.
- [39] T. Lu, F. Chen, Multiwfn: a multifunctional wavefunction analyzer, *J. Comput. Chem.* 33 (5) (2012) 580–592, <https://doi.org/10.1002/jcc.22885>.
- [40] N.M. O'Boyle, A.L. Tenderholt, K.M. Langner, cclib: a library for package-independent computational chemistry algorithms, *J. Comput. Chem.* 29 (5) (2008) 839–845, <https://doi.org/10.1002/jcc.20823>.
- [41] T. Swift, L. Swanson, M. Geoghegan, S. Rimmer, The pH-responsive behaviour of poly(acrylic acid) in aqueous solution is dependent on molar mass, *Soft Matter* 12 (9) (2016) 2542–2549, <https://doi.org/10.1039/C5SM02693H>.
- [42] A. Kyrchenko, M.M. Blazhynska, M.V. Slavgorodska, O.N. Kalugin, Stimuli-responsive adsorption of poly(acrylic acid) onto silver nanoparticles: Role of polymer chain length and degree of ionization, *J. Mol. Liq.* 276 (2019) 243–254, <https://doi.org/10.1016/j.molliq.2018.11.130>.
- [43] Y.T. Tao, Structural comparison of self-assembled monolayers of n-alkanoic acids on the surfaces of silver, copper, and aluminum, *J. Am. Chem. Soc.* 115 (10) (1993) 4350–4358, <https://doi.org/10.1021/ja00063a062>.
- [44] A. Gole, S.R. Sainkar, M. Sastry, Electrostatically controlled organization of carboxylic acid derivatized colloidal silver particles on amine-terminated self-assembled monolayers, *Chem. Mater.* 12 (5) (2000) 1234–1239, <https://doi.org/10.1021/cm990439u>.
- [45] B. Parker, B. Immaraporn, A.J. Gellman, Carboxylic acid deprotonation on the Ag (110) and Ag(111) surfaces, *Langmuir* 17 (21) (2001) 6638–6646, <https://doi.org/10.1021/la011103d>.
- [46] I.C. McNeill, S.M.T. Sadeghi, Thermal stability and degradation mechanisms of poly(acrylic acid) and its salts: Part 1—Poly(acrylic acid), *Polym. Degrad. Stab.* 29 (2) (1990) 233–246, [https://doi.org/10.1016/0141-3910\(90\)90034-5](https://doi.org/10.1016/0141-3910(90)90034-5).
- [47] S. Milardović, I. Ivanišević, A. Rogina, P. Kassal, Synthesis and electrochemical characterization of AgNP ink suitable for inkjet printing, *Int. J. Electrochem. Sci.* 13 (11) (2018) 11136–11149, <https://doi.org/10.20964/2018.11.87>.
- [48] V.T. Trinh, T.M.P. Nguyen, H.T. Van, L.P. Hoang, T.V. Nguyen, L.T. Ha, X.H. Vu, T. T. Pham, T.N. Nguyen, N.V. Quang, X.C. Nguyen, Phosphate adsorption by silver nanoparticles-loaded activated carbon derived from tea residue, *Sci. Rep.* 10 (1) (2020) 3634, <https://doi.org/10.1038/s41598-020-60542-0>.
- [49] S. Mukherji, S. Bharti, G. Shukla, S. Mukherji, Synthesis and characterization of size- and shape-controlled silver nanoparticles, *Phys. Sci. Rev.* 4 (1) (2019), <https://doi.org/10.1515/psr-2017-0082>.
- [50] A. Liebsch, Surface-plasmon dispersion and size dependence of Mie resonance: Silver versus simple metals, *Phys. Rev. B* 48 (15) (1993) 11317–11328, <https://doi.org/10.1103/PhysRevB.48.11317>.
- [51] C.M. Ho, S.K. Yau, C.N. Lok, M.H. So, C.M. Che, Oxidative dissolution of silver nanoparticles by biologically relevant oxidants: a kinetic and mechanistic study, *Chem. Asian J.* 5 (2) (2010) 285–293, <https://doi.org/10.1002/asia.200900387>.
- [52] S. Garg, H. Rong, C.J. Miller, T.D. Waite, Oxidative dissolution of silver nanoparticles by chlorine: implications to silver nanoparticle fate and toxicity, *Environ. Sci. Technol.* 50 (7) (2016) 3890–3896, <https://doi.org/10.1021/acs.est.6b00037>.
- [53] L.E. Valenti, C.E. Giacomelli, Stability of silver nanoparticles: agglomeration and oxidation in biological relevant conditions, *J. Nanopart. Res.* 19 (5) (2017) 156, <https://doi.org/10.1007/s11051-017-3860-4>.
- [54] B. Molleman, T. Hiemstra, Surface structure of silver nanoparticles as a model for understanding the oxidative dissolution of silver ions, *Langmuir* 31 (49) (2015) 13361–13372, <https://doi.org/10.1021/acs.langmuir.5b03686>.
- [55] S.W. Cranford, M.J. Buehler, Critical cross-linking to mechanically couple polyelectrolytes and flexible molecules, *Soft Matter* 9 (4) (2013) 1076–1090, <https://doi.org/10.1039/C2SM27055B>.
- [56] S. Simon, M. Duran, J.J. Dannenberg, How does basis set superposition error change the potential surfaces for hydrogen-bonded dimers? *J. Chem. Phys.* 105 (24) (1996) 11024–11031, <https://doi.org/10.1063/1.472902>.
- [57] M. Gray, P.E. Bowling, J.M. Herbert, Systematic evaluation of counterpoise correction in density functional theory, *J. Chem. Theory Comput.* 18 (11) (2022) 6742–6756, <https://doi.org/10.1021/acs.jctc.2c00883>.
- [58] V.S. Bryantsev, M.S. Diallo, A.C.T. van Duin, W.A. Goddard, III, Evaluation of B3LYP, X3LYP, and M06-class density functionals for predicting the binding energies of neutral, protonated, and deprotonated water clusters, *J. Chem. Theory Comput.* 5 (4) (2009) 1016–1026, <https://doi.org/10.1021/ct800549f>.
- [59] I. Tordjman, A. Boudjada, J.-C. Guitel, R. Masse, Structure de l'hydrogenophosphate d'argent Ag₂HPO₄, *Acta Crystallogr. Sect. B* 34 (12) (1978) 3723–3725, <https://doi.org/10.1107/S0567740878011966>.
- [60] S. Cui, L. Huang, Q. Li, H. Hu, W. Feng, Pressure-induced phase transition of AgClO₄: a first-principles study, *Solid State Commun.* 165 (2013) 1–5, <https://doi.org/10.1016/j.ssc.2013.04.004>.
- [61] S. Dapprich, G. Frenking, Investigation of donor-acceptor interactions: a charge decomposition analysis using fragment molecular orbitals, *J. Phys. Chem.* 99 (23) (1995) 9352–9362, <https://doi.org/10.1021/j100023a009>.
- [62] G. Frenking, U. Pidun, Ab initio studies of transition-metal compounds: the nature of the chemical bond to a transition metal, *J. Chem. Soc. Dalton Trans.* (10) (1997) 1653–1662, <https://doi.org/10.1039/A700329C>.
- [63] C.-G. Zhan, J.A. Nichols, D.A. Dixon, Ionization potential, electron affinity, electronegativity, hardness, and electron excitation energy: molecular properties from density functional theory orbital energies, *J. Phys. Chem. A* 107 (20) (2003) 4184–4195, <https://doi.org/10.1021/jp0225774>.
- [64] S. Srinivas, U.A. Salián, J. Jellinek, Theoretical Investigations of Silver Clusters and Silver-Ligand Systems, in: N. Russo, D.R. Salahub (Eds.), *Metal-Ligand Interactions in Chemistry, Physics and Biology*, Springer Netherlands, Dordrecht, 2000, pp. 295–324, https://doi.org/10.1007/978-94-011-4245-8_12.
- [65] A. Panáček, R. Prucek, J. Hrbáč, T.J. Nevečná, J. Steffková, R. Zbořil, L. Kvítek, Polyacrylate-assisted size control of silver nanoparticles and their catalytic activity, *Chem. Mater.* 26 (3) (2014) 1332–1339, <https://doi.org/10.1021/cm400635z>.
- [66] M.L. McKee, A. Samokhvalov, Density functional study of neutral and charged silver clusters Ag-n with n=2–22. Evolution of properties and structure, *J. Phys. Chem. A* 121 (26) (2017) 5018–5028, <https://doi.org/10.1021/acs.jpca.7b03905>.